Journal of Alloys and Compounds 480 (2009) 321–324

Contents lists available at ScienceDirect

Journal of Alloys and Compounds

journal homepage: www.elsevier.com/locate/jallcom

Hydrogenation of Zr–Cu–Al–Ni–Pd metallic glasses by electrochemical means

N. Ismail [a,*], A.A. El-Meligi [a], M. Uhlemann [b], A. Gebert [b], J. Eckert [b], L. Schultz [b]

[a] Physical Chemistry Department, National Research Centre, Cairo, PO Box 12311, Egypt
[b] IFW Dresden, Institut für Metallische Werkstoffe, Postfach 270016, D-01171 Dresden, Germany

ARTICLE INFO

Article history:
Received 20 August 2008
Received in revised form 29 January 2009
Accepted 30 January 2009
Available online 10 February 2009

Keywords:
Electrochemical hydrogenation
Thermal desorption
Thermal stability
Zr-based metallic glasses

ABSTRACT

Amorphous materials of Zr–Cu–Ni–Al systems have shown attractive electrochemical hydrogen absorption properties. A comparison between $Zr_{60}Cu_{15}Al_{10}Ni_{10}Pd_5$ and $Zr_{65}Cu_{17.5}Al_{7.5}Ni_{10}$ reveals that the palladium (Pd) increases the hydrogen absorption capacity. Charging melt-spun $Zr_{60}Cu_{15}Al_{10}Ni_{10}Pd_5$ ribbons electrochemically to different hydrogen-to-metal (H/M) ratios and following the effusion of hydrogen by thermal desorption analysis (TDA) reveals hydrogen desorption from interstitial sites of high energy levels at temperatures below 630 K. Zirconium hydrides are formed above 630 K. At higher temperatures partial desorption of hydrogen occurs. The thermal stability observed with differential scanning calorimetry (DSC) of the amorphous phase has been significantly deteriorated by hydrogen absorption. After hydrogenation, the crystallization behaviour shows suppression of the characteristic quasicrystalline phase and depends on the hydrogen content. Therefore, at low hydrogen concentrations H/M = 0.3, Cu and/or Cu-rich phases are primarily formed while at high hydrogen concentrations H/M ≥ 0.9 Zr-hydride phase(s) are mainly formed.

1. Introduction

Selected Zr–Cu–Al–Ni metallic glasses systems exhibit a wide under-cooled liquid region corresponding to a high thermal stability and high glass forming ability. The Zr-base alloys are amorphous materials with excellent mechanical properties such as low Young's modulus, high specific strength and good chemical resistivity [1,2], which are especially prominent for several industrial needs as well as medical applications [3]. Recently, a completely new application of Zr-base alloys have been developed at California Institute of Technology [4], in which the material with composition, $Zr_{58.5}Cu_{15.6}Ni_{12.8}Al_{10.3}Nb_{2.8}$ (Vitreloy 106a), is used as a collector for solar noble gases on NASA's Genesis mision [5,6]. These properties have encouraged a lot of different investigations in order to explore the benefits and the advantages of that system [7–11]. The presences of early and late transition metals (ETM/LTM) in the alloy composition which have a different affinity towards hydrogen make these compounds interesting candidates for hydrogenation studies. Hydrogen can be used as a probe to explore the structure of metallic glassy alloys and the structure distribution of interstitial sites [12]. Neutron diffraction studies for binary Zr–Ni metallic glasses showed that hydrogen favours tetrahedra structure units with four Zr atoms, which have the highest affinity towards hydrogen followed by tetrahedra with three Zr atoms and one Ni [13]. A statistical model suggested a chemically random alloy with a structure consisting of packed, distorted tetrahedral [14]. Previous investigations proved that Zr–Cu–Al–Ni metallic glass as prepared by melt spinning are able to store hydrogen electrochemically up to maximum values between 1.3 H/M and 1.6 H/M (H/M is the hydrogen/metal ratio) depending on the alloy composition [15–17]. These values are comparable to those of Ti–Zr–Ni(Cu) quasicrystalline and amorphous alloys, which the authors consider as promising hydrogen storage materials [18–21].

In this paper, we studied the effect of the addition of palladium (Pd) to a Zr–Cu–Al–Ni metallic glass system on the hydrogenation properties. The Pd had been chosen since it is known to have high affinity towards hydrogen absorption. We present a detailed study on electrochemical hydrogenation and its effect on the thermal stability and crystallization behaviour of the amorphous alloy.

2. Experimental

$Zr_{60}Cu_{15}Al_{10}Ni_{10}Pd_5$ and $Zr_{65}Cu_{17.5}Al_{7.5}Ni_{10}$ were prepared by arc melting Zr, Al, Cu, Ni and Pd with a purity of 99.9% in argon atmosphere. For high homogeneity the samples were remelted several times. From the master alloys, ribbons of 40 μm thickness were prepared in a single-roller Bühler melt spinner under argon condition.

The ribbons were polished by emery paper of 600-grade before cathodically charged in an electrolytic solution of 0.1 M NaOH containing 5×10^{-5} mol/l As_2O_3 as a surface-poisoner for atomic hydrogen absorption. The current density applied was −1, −10 and −20 mA/cm^2 for different time intervals. The hydrogen content was measured by hydrogen determinator (LECO 402). The T-dependent effusion of hydrogen was monitored with a thermal desorption analyser (TDA) in ultra high vacuum chamber (UHV) by heating the charged ribbons till 750 °C using heating rate of 15 K/min.

* Corresponding author.
E-mail address: nahlaismail24@yahoo.com (N. Ismail).

0925-8388/$ – see front matter.
doi:10.1016/j.jallcom.2009.01.138

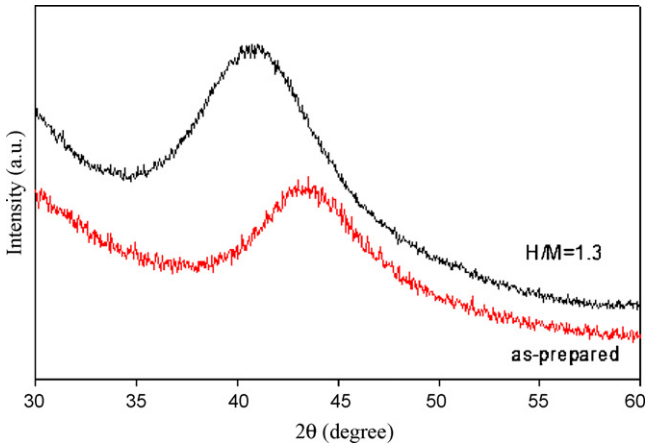

Fig. 1. XRD pattern of as-quenched and hydrogen-charged $Zr_{60}Cu_{15}Al_{10}Ni_{10}Pd_5$ metallic glass (H/M = 1.3) at room temperature.

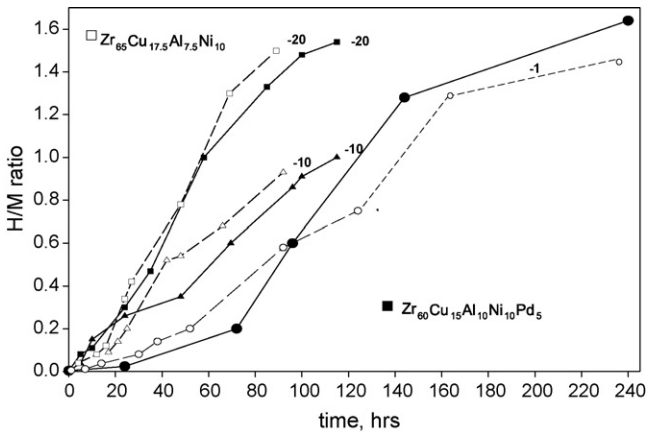

Fig. 2. Results of galvanostatic charging of amorphous $Zr_{60}Cu_{15}Al_{10}Ni_{10}Pd_5$ (solid points and solid lines) and $Zr_{65}Cu_{17.5}Al_{7.5}Ni_5$ (hallow points and dashed lines), using current densities of −1, −10 and −20 mA/cm^2.

The thermal stability was studied by means of differential scanning calorimeter, Perkin Elmer DSC7 at constant heating rate of 20 K/min. X-ray diffraction (XRD) patterns were recorded by Philips PW 1050 diffractometer with Co Kα radiation. It was used for phase analysis at room temperature after heating charged and as-quenched ribbons at constant heating rate of 15 K/min to selected temperatures. Auger electron spectroscopy (AES) sputter profiling was used to investigate the composition of the alloy surface. The analysis was performed with a PHI 660 Auger microprobe applying 10 keV as primary energy, 100 nA electron current. Depth profiling was done by sputtering using argon ions at 60° to the sample normal with an energy of E = 1.5 keV.

3. Results and discussion

3.1. Characteristics of the hydrogenated samples at room temperature

Fig. 1 shows XRD patterns for an as-quenched $Zr_{60}Cu_{15}Al_{10}Ni_{10}Pd_5$ ribbon and for a ribbon after electrochemical hydrogen charging to H/M = 1.3. Although hydrogen embrittles the ribbon, the alloy remains amorphous upon charging. However, the broad maxima characteristic of the amorphous state shift to lower 2θ value of about 39° in comparison to the uncharged alloy of about 44°, indicating an expansion of the amorphous structure upon hydrogen uptake. When charging to high H/M ratio, the brightness of the ribbons surface turns darker and duller. The surface compositions of the $Zr_{60}Cu_{15}Al_{10}Ni_{10}Pd_5$ alloy charged up to H/M = 0.9 and H/M = 1.3 under a charging current density of −20 mA/cm^2 was investigated by AES measurements. The surface of the charged samples was found to be altered significantly compared with the as-prepared one. The naturally formed oxide layer is highly reduced. It is known that the air-exposed surfaces of Zr-base alloys are covered with the thin protective oxide layer [22,23]. A depletion of the Zr concentration and enrichment of Cu and Al are always detected on the surface of the charged samples. The depletion of the Zr concentration can be explained by the possible formation of fine Zr-hydride crystallites on the amorphous matrix as it was observed before for $Zr_{65}Cu_{17.5}Al_{7.5}Ni_5$ amorphous ribbons [16]. This means that hydrogen induces locally at the surface changes in the atomic arrangement of the amorphous phase in order to increase the number of sites with highest affinity to hydrogen, i.e. Zr sites.

Charging both amorphous ribbon samples with hydrogen using a low current density of −1 mA/cm^2 till the maximum capacity at which the ribbons lose completely its ductility, i.e. undergo self-degradation, the $Zr_{60}Cu_{15}Al_{10}Ni_{10}Pd_5$ gives higher maximum hydrogen capacity of H/M = 1.78 after nearly one month than the $Zr_{65}Cu_{17.5}Al_{7.5}Ni_{10}$ which gives maximum hydrogen capacity of H/M = 1.65. This is explained on the basis that Pd has high affinity towards hydrogen absorption which increases the number of interstitial sites, and disordered octahedral structure. It is known that hydrogen prefers to occupy the octahedral structure [14]. By observation, the amorphous ribbon containing Pd is able to reserve its ductility longer time than the sample without Pd. Using higher charging rates of −10 and −20 mA/cm^2, both ribbons lose its ductility in a shorter time and before they reach the maximum hydrogen absorption capacity. Yet still the sample with Pd can reserve its ductility longer than the sample without Pd.

Fig. 2 represents the hydrogen absorption rates of $Zr_{65}Cu_{17.5}Al_{7.5}Ni_{10}$ and $Zr_{60}Cu_{15}Al_{10}Ni_{10}Pd_5$. Generally, the hydrogen absorption rate of $Zr_{60}Cu_{15}Al_{10}Ni_{10}Pd_5$ alloy is slower than the alloy without Pd. As observed, the $Zr_{65}Cu_{17.5}Al_{7.5}Ni_{10}$ and $Zr_{60}Cu_{15}Al_{10}Ni_{10}Pd_5$ rate of hydrogen absorption is slow when applying low current density (−1 and −10 mA/cm^2) up to about 75 h. This may be due to presence of thick oxide layer. After 75 h of applying current density, the rate of hydrogen charging for the $Zr_{60}Cu_{15}Al_{10}Ni_{10}Pd_5$ alloy is slower than $Zr_{65}Cu_{17.5}Al_{7.5}Ni_{10}$. This is may be due to fast reduction of the oxide layer, also, may be due to surface activation process of the $Zr_{65}Cu_{17.5}Al_{7.5}Ni_{10}$ alloy for hydrogen absorption is slower than $Zr_{60}Cu_{15}Al_{10}Ni_{10}Pd_5$ alloy.

At high current density, −20 mA/cm^2, the rate of hydrogen charging for both alloys is fast. This is may be due to fast reduction of the oxide layer. The presence of oxide film on the Zr-base alloys was proved [3,22,23]. It was stated that all elements of the Zr-base alloys are present in the oxide layer, but in different stoichiometric composition as compared to the composition of the Zr-base alloy itself. Based on the XPS measurements by Homazava et al. the oxide film consists mainly of ZrO_2 with a smaller fraction of Al_2O_3 and very small amounts of Cu, Ni and Pd-oxides [3].

3.2. Thermal stability of the hydrogenated alloy

Fig. 3 displays thermal desorption curves for $Zr_{60}Cu_{15}Al_{10}Ni_{10}Pd_5$ sample with different H/M values. The desorption can be divided into two different stages, first one is below 635 K and a second stage starts after 660 K which is characterized by the appearance of successive desorption peaks. Ribbons with low and medium H/M ratios of 0.15 and 0.6, respectively (Fig. 3, curves c and b) show no hydrogen effusion in the first temperature range below 630 K, indicating that the hydrogen is captured in interstitial sites with tetrahedral and octahedral symmetry corresponding to low energy levels with high affinity to hydrogen [18,13]. In contrast, the sample with the high hydrogen content of H/M = 0.95 shows a broad desorption band which starts at about 460 K and drops to nearly the base line at 630 K (Fig. 3,

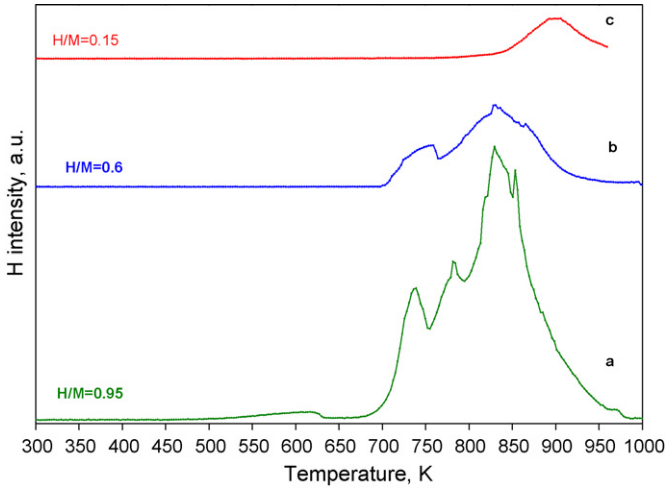

Fig. 3. Thermal desorption analysis of hydrogen-charged $Zr_{60}Cu_{15}Al_{10}Ni_{10}Pd_5$ metallic glass with different hydrogen contents performed at a heating rate of 15 K/min.

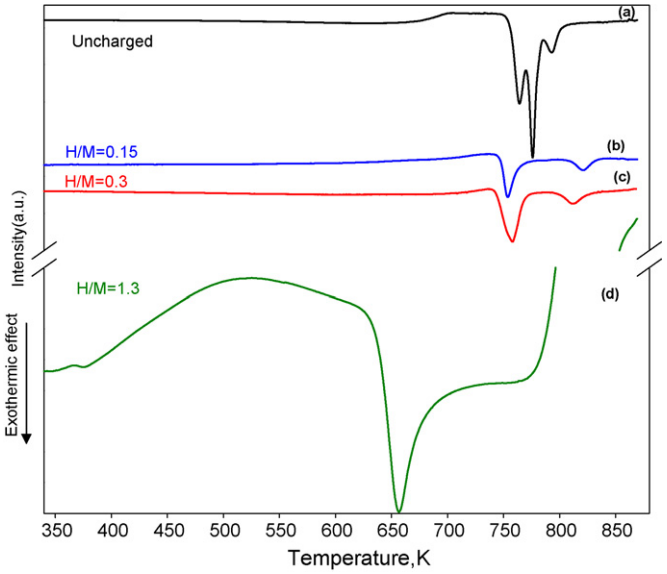

Fig. 4. DSC measurements of hydrogen-charged $Zr_{60}Cu_{15}Al_{10}Ni_{10}Pd_5$ metallic glass with different hydrogen contents performed at a heating rate of 20 K/min.

curve a). This broad band points to hydrogen desorption from interstitial sites of high energy level [14,17]. At 630 K a drop of the broad curve occurs, reaching nearly the level of the baseline. At this temperature, the remaining hydrogen has reacted to crystalline Zr-hydride phases as proved by XRD (see Fig. 5c). The desorption behaviour of the second range at temperatures above 673 K is characteristic for partial decomposition and transformation of different hydride crystalline phases and effusion of hydrogen upon decomposition [17]. The different steps of decomposition and phase transformation cannot be systematically investigated for the samples with H/M ratio 0.6 and 0.95. This may be due to the crystallization of the quinary alloy included different hydride phases of Zr, Ni and Pd, which overlapped during hydrogen effusion. Although the XRD patterns showed only Zr-hydride phases, the formation of Ni and Pd hydride phases are possible but the limits of there crystallites concentrations could not be detected. Fig. 3c of a sample with low hydrogen concentration (H/M = 0.15) shows that hydrogen effusion begins at about 823 K due to the decomposition of $(\alpha+\beta)$ Zr-hydride phase mixture. This result is in agreement with Zr-H phase diagram which indicated the formation of α hydrides or $(\alpha+\beta)$ Zr-hydrides at low hydrogen concentrations and its effusion at about 813 K [24].

The change in the thermal stability of the $Zr_{60}Cu_{15}Al_{10}Ni_{10}Pd_5$ metallic glass by the absorption of different amounts of hydrogen is shown in Fig. 4. Curve (a) represents the thermal behaviour of the uncharged alloy. The differential scanning calorimetry (DSC) scan exhibits a distinct endothermic heat effect due to the glass transition followed by a sharp exothermic peak corresponding to the crystallization of the material. The glass transition temperature T_g determined as the onset temperature of the endotherm is 672 K and the onset of crystallization occurs at T_x = 754 K, leading to a rather wide supercooled liquid region $\Delta T_x = T_x - T_g$ of 82 K for the heating rate of 20 K/min. This is followed by three characteristic successive crystallization peaks. The first peak corresponds to the formation of metastable quasicrystalline phase and the next two peaks correspond to the subsequent transformation to the equilibrium phases.

The formation of the quasicrystalline phase at the onset crystallization temperature is evident from the XRD pattern in Fig. 5a. Absorption of small amounts of hydrogen, H/M = 0.15, significantly reduces the thermal stability of the ribbons as illustrated in curve 5b so that the crystallization temperature decreases to 742 K and the glass transition temperature shifts to higher temperatures resulting in a reduction of the under-cooled liquid region ΔT_x to 34 K. More hydrogen concentration in the amorphous matrix continues to decrease the crystallization temperature as clearly seen in curve 5c for H/M = 0.3. The sequences of crystallization peaks seem to change greatly by hydrogen absorption compared with the uncharged sample. For samples of H/M = 0.15 and 0.3 two non-successive crystallization peaks occur. From the XRD pattern of the ribbon charged with H/M = 0.3 and heated till the onset temperature of crystallization T_x = 741 K, it is obvious that the crystallization process changed significantly. The formation of the quasicrystalline phase is suppressed, instead, crystallization occur via the formation of nanocrystalline Cu and/or Cu-rich phases, such as cubic Cu_4Al and Cu_9Al_4 (see Fig. 5b). This result can be explained in terms with the enrichment of Cu and depletion of Zr on the charged ribbon surface detected by AES measurements which may enhance the crystallization of Cu and/or Cu-rich phases as the starting phases of crystallization. This result agrees with the results studied in details before for $Zr_{65}Cu_{17.5}Al_{7.5}Ni_{10}$ alloy [16]. The second exothermic peaks detected at 820 K for H/M = 0.15 and shifted to 813 K for

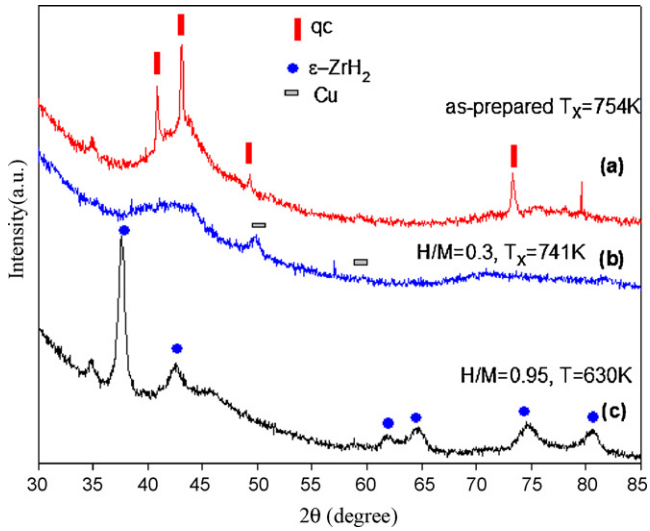

Fig. 5. XRD analysis of annealed as prepared and hydrogen-charged $Zr_{60}Cu_{15}Al_{10}Ni_{10}Pd_5$ metallic glass at different conditions.

higher hydrogen concentration H/M = 0.3 are due to partial transformation to ($\alpha + \beta$) Zr-hydrides at low hydrogen concentrations. This result agrees with the Zr-H phase diagram [24].

For high hydrogen contents, e.g. H/M $\geq$ 0.9 (Fig. 4, curve d), only the formation of the Zr-hydride is detected. The strong exothermic event starting at 630 K is due to the formation of ε-Zr-hydride, most likely with different stoichiometrices, which is also shown (Fig. 3, curve a) by TDA and clearly identified by XRD pattern in Fig. 5c. After that a strong endothermic effect starts after 760 K due to the hydrogen desorption. There are no signs for exothermic reactions upon crystallization of amorphous matrix, as in this case the summation of the exothermic crystallization and the endothermic reaction for decomposition of a large amount of Zr-hydride phases is endothermic.

4. Conclusions

- At room temperature $Zr_{60}Cu_{15}Al_{10}Ni_{10}Pd_5$ metallic glass alloy has maximum hydrogen capacity than $Zr_{65}Cu_{17.5}Al_{7.5}Ni_{10}$. But the hydrogen absorption rate of $Zr_{60}Cu_{15}Al_{10}Ni_{10}Pd_5$ is slower than $Zr_{65}Cu_{17.5}Al_{7.5}Ni_{10}$, especially, during early period of applying current density (up to 75 h). The presence of oxide film on the Zr-base alloys affects the hydrogen absorption rate under different current densities.
- Hydrogen absorption causes enrichment of the elements of very low affinity towards hydrogen on the alloy surface, e.g. Cu, and depletion of the elements of high affinity on the surface, e.g. Zr.
- The thermal stability and the crystallization behaviour of the Zr-based metallic glass strongly depend on the amount of hydrogen in the alloy. Already small amounts of hydrogen in the amorphous alloy cause a deterioration of its thermal stability, i.e. a diminution of the supercooled liquid region mostly resulting from a decrease of the crystallization temperature and suppresses the formation of metastable quasicrystalline phase. At low hydrogen contents, Cu and/or Cu-rich phases are the primary crystalline phases while at high hydrogen contents the thermal stability of the alloy is determined by Zr-hydride formation.

References

[1] A. Inoue, Bulk Amorphous Alloys: Practical Characteristics and Applications, Trans Tech Publications, 1999.
[2] W.H. Wang, C. Dong, C.H. Shek, Material Science and Engineering R 44 (2004) 45–89.
[3] N. Homazava, A. Shkabko, D. Logvinovich, U. Krâhenbühl, A. Ulrich, Intermetallics (2008) 1–7.
[4] C.C. Hays, J. Schroers, U. Geyer, S. Bossuyt, N. Stein, W.L. Johnson, Material Science Forum 343–346 (2000) 103–108.
[5] A. Grimberg, H. Baur, P. Bochsler, F. Buâhler, D.S. Burnett, C.C. Hays, Science 314 (2006) 1133–1135.
[6] A. Grimberg, H. Baur, F. Bühler, P. Bochsler, R. Wieler, Geochimica Cosmochimica Acta 72 (2008) 626–645.
[7] N. Van Steenberge, J. Sort, A. Concustell, J. Das, S. Scudino, S. Surinach, J. Eckert, M.D. Baró, Scripta Materialia 56 (2007) 605–608.
[8] S. Scudino, J. Eckert, H. Breitzke, K. Lüders, L. Schultz, Materials Science and Engineering A 449–451 (2007) 493–496.
[9] S. Scudino, J. Eckert, X.Y. Yang, D.J. Sordelet, L. Schultz, Intermetallics 15 (2007) 571–582.
[10] S. Bossuyt, S.V. Madge, G.Z. Chena, A. Castellero, S. Deledda, J. Eckert, D.J. Fray, A.L. Greer, Materials Science and Engineering A 375–377 (2004) 240–243.
[11] U. Kamachi Mudali, S. Baunack, J. Eckert, L. Schultz, A. Gebert, Journal of Alloys and Compounds 377 (2004) 290–297.
[12] U. Stolz, R. Kirchheim, A. Wildermuth, Rapidly Quenched Metals (1985) 1537.
[13] K. Suzuki, N. Hayashi, Y. Tomizuka, T. Fukunaga, K. Kai, N. Watanabe, Journal of Non-Crystalline Solids 61 (62) (1984) 637.
[14] J.H. Harris, W.A. Curtin, M. Tenhover, Physical Review B 36 (1997) 5984.
[15] A. Gebert, N. Ismail, M. Uhlemann, J. Eckert, L. Schultz, Intermetallics 10 (2002) 1207–1213 (Nr. 11-12, S).
[16] N. Ismail, A. Gebert, M. Uhlemann, J. Eckert, L. Schultz, Journal of Alloys and Compounds 314 (2001) 170–176 (Nr. 1-2. S).
[17] N. Ismail, M. Uhlemann, A. Gebert, J. Eckert, Journal of Alloys and Compounds 298 (2000) 146–152 (Nr. 1-2, S).
[18] J.Y. Kim, R. Hennig, V.T. Huett, P.C. Gibbons, K.F. Kelton, Journal of Alloys and Compounds 404–406 (2005) 388–391.
[19] A.D. Ruda, U. Schmidt, G.M. Zelinska, A.M. Lakhnik, A.E. Perekos, G.Y. Kolbasov, M.O. Danilov, Journal of Alloys and Compounds 404–406 (2005) 515–518.
[20] B. Liu, D. Liu, Y. Wu, L. Li, L. Wang, International Journal of Hydrogen Energy 32 (2007) 2429–2433.
[21] B. Liu, Y. Wu, L. Wang, Journal of Power Sources 162 (2006) 713–718.
[22] A. Dhawan, V. Zaporojtchenko, F. Faupel, S.K. Sharma, Journal of Material Science 42 (2007) 9037–9044.
[23] S.K. Sharma, T. Strunskus, H. Ladebusch, F. Faupel, Material Science and Engineering A 304–306 (2001) 747–752.
[24] T.B. Massalski, Binary Alloys Phase Diagram, 2nd edition, Materials Park, Ohio: ASM International, 1992, p. 2078.